Quantum Optical Signatures in a Strong Laser Pulse after Interaction with Semiconductors

N. Tsatrafyllis,[1] S. Kühn,[2] M. Dumergue,[2] P. Foldi,[2,3] S. Kahaly,[2] E. Cormier,[2,4] I. A. Gonoskov,[5] B. Kiss,[2] K. Varju,[2,6] S. Varro,[2,7] and P. Tzallas[1,2,*]

[1]*Foundation for Research and Technology-Hellas, Institute of Electronic Structure and Laser, PO Box 1527, GR-71110 Heraklion, Greece*

[2]*ELI-ALPS, ELI-Hu Non-Profit Ltd., Dugonics tér 13, H-6720 Szeged, Hungary*

[3]*Department of Theoretical Physics, University of Szeged, Dom ter 9, 6720 Szeged, Hungary*

[4]*Univ Bordeaux, CNRS, CELIA, CEA, F-33405 Talence, France*

[5]*Max Planck Institute of Microstructure Physics, Weinberg 2, D-06120 Halle, Germany*

[6]*Department of Optics and Quantum Electronics, University of Szeged, Dom ter 9, 6720 Szeged, Hungary*

[7]*Wigner Research Center for Physics, 1121 Budapest, Hungary*

(Received 28 September 2018; published 14 May 2019)

Electrodynamical processes induced in complex systems like semiconductors by strong electromagnetic fields have traditionally been described using semiclassical approaches. Although these approaches allowed the investigation of ultrafast dynamics in solids culminating in multipetahertz electronics, they do not provide any access to the quantum-optical nature of the interaction, as they treat the driving field classically and unaffected by the interaction. Here, using a full quantum-optical approach, we demonstrate that the subcycle electronic response in a strongly driven semiconductor crystal is imprinted in the quantum state of the driving field resulting in nonclassical light states carrying the information of the interaction. This vital step towards strong-field ultrafast quantum electrodynamics unravels information inaccessible by conventional approaches and leads to the development of a new class of nonclassical light sources.

DOI: 10.1103/PhysRevLett.122.193602

Over the past decades, semiconductor quantum optics [1] has led to fascinating discoveries in the field of quantum technology [2] with nonclassical light sources [3–11] playing an essential role in these research directions. Most of these investigations have been performed using weak electromagnetic fields where the interaction can be described by fully quantized theories that treat both the field and the interaction quantum mechanically allowing the field to be affected by the interaction. On the other hand, in the recent past, the interaction of semiconductor crystals with strong electromagnetic fields has attracted keen interest. This is because it combines the advantages of electronics and attosecond physics [12]. The fundamental mechanism underlying such interactions relies on the sub-laser-cycle electron dynamics induced in the crystal lattice by the strong field of the driving laser. Untangling this subcycle dynamics led to pioneering discoveries in ultrafast solid-state physics and attosecond optoelectronics [13–17]. Nevertheless, these studies remain disconnected from the quantum technology roadmap [2], because, due to the high photon number of the driving field, the interaction is described using semiclassical theories treating the driving laser field classically, i.e., without considering its quantum nature, and therefore missing any imprint of the interaction encoded on the quantum state of the light. Here, using a full quantum-optical approach, we reveal the subcycle quantum electrodynamics of the interaction and we show that the quantum state of the light exiting the crystal depicts nonclassical features carrying the subcycle information of the interaction. This has been achieved using the high harmonics (HH) generated by the interaction of crystalline zinc oxide (ZnO) with intense midinfrared (mid-IR) laser pulses.

According to semiclassical theories [12,18–28], the generation of HH of order q in the strong-field region relies on a subcycle nonlinear process which is dominated by the dynamics of interband transitions. An intuitive physical picture of the process can be given using the concept of the electron trajectories as is shown in Figs. 1(a) and 1(b). When an intense linearly polarized laser field (with photon energy much lower than the energy band gap of the material) interacts with a crystal, the electron escapes the valence band to the conduction band, it subsequently accelerates in the conduction band (likewise the hole in the valence band) gaining energy from the driving field, and recombines with the hole (in a multicenter recombination process along the crystal lattice) within the same cycle of the driving field. This recombination process generates radiation with frequencies higher than the driving field and, for multicycle interactions, leads to the emission of HH in the visible-UV region. The term "recombination" was used according to the terminology of Refs. [18–23,26,28].

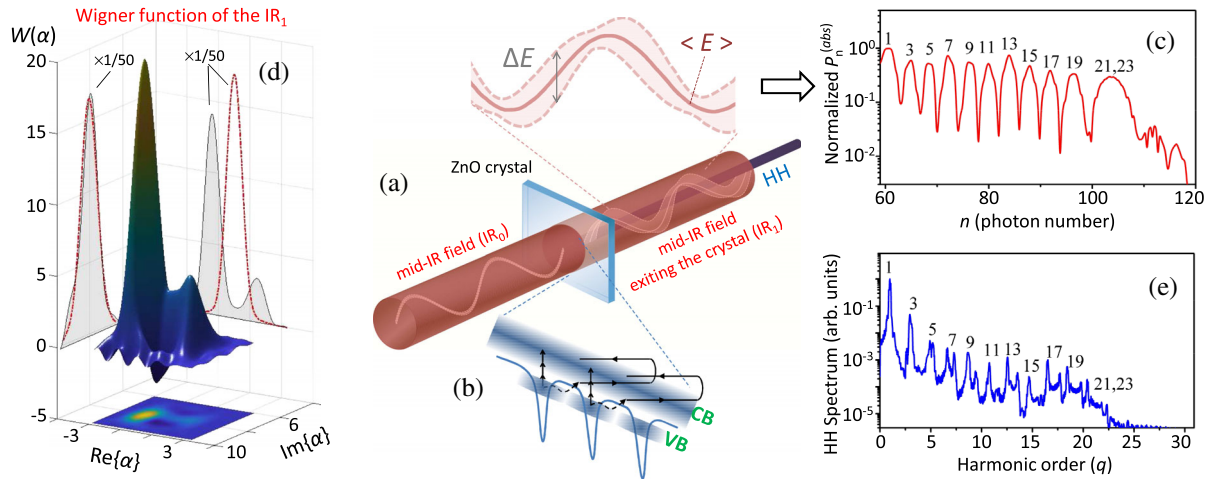

FIG. 1. (a) Schematic of the interaction of the mid-IR pulses with the ZnO crystal. The pink shaded area of the mid-IR field before and after the interaction reflects the electric field variance (ΔE) as has been calculated by the theoretical model. The blue beam shows the HH beam after the crystal. (b) A simplified schematic representation of the multiphoton and interband transitions in a periodic potential induced by an intense mid-IR laser-field. (c) Distribution of the probability to absorb mid-IR photons towards harmonic emission ($P_n^{(abs)}$) calculated using the theoretical model. (d) $W(a)$ (shown at the field phase $\theta = 3\pi/2$) of the mid-IR field exiting the medium and the corresponding marginal distributions (gray filled areas). The $W(a)$ is moving on a circle in phase space with $|\alpha|^2$ the photon number expectation value. For reasons of comparison, we provide the marginal distributions (red dashed lines) of a coherent state with the same $|\alpha|^2$. Its deviation from coherent states clearly depicts the nonclassical character of the light state exiting the medium. (e) Calculated HH spectrum. This spectrum has no distinguishable difference compared to the HH spectrum calculated using the semiclassical version of the theoretical model.

Although the above theories can sufficiently describe the HH generation process, they do not provide any access to the backaction of the process on the quantum state of the driving laser field.

To unravel the influence of the subcycle nonlinear process on the quantum state of the driving laser field, we have calculated and measured the photon number distribution of the mid-IR laser field exiting the crystal by utilizing the UV–mid-IR anticorrelation approach (named hereafter "quantum spectrometer") that has been demonstrated for gases [29].

To gain insight on the quantum electrodynamics of the system, we have extended the semiclassical theoretical approach described in Ref. [25] to the quantum-optical regime. The model [Supplemental Material (SM) [30], Pt. 1] describes in 1D the main features of the interaction using a quantized mid-IR laser field. The Hamiltonian of the interaction in the dipole approximation is

$$H = \hbar\omega_L\left(\alpha_L^+\alpha_L + \frac{1}{2}\right) + \sum_q \hbar\omega_q\left(\alpha_q^+\alpha_q + \frac{1}{2}\right) + \frac{1}{2m_e}[\boldsymbol{p} - e\boldsymbol{A}]^2 + U(\boldsymbol{r}),$$

where e and m_e are the charge and the mass of the electron and ω_L and ω_q are the frequencies of the driving laser field and the harmonics, respectively. Electron-electron interactions are neglected. The first and second terms describe the free-quantized mid-IR (single-mode) and HH fields, the third term describes the light-matter coupling [in velocity gauge, $A = \sqrt{\hbar/2\omega_L\varepsilon_0 V}(\alpha + \alpha^+)$, with α^+ and α being the creation and annihilation operators and V the quantization volume], while the spatial coordinate is introduced in $U(\boldsymbol{r})$, which describes the lattice periodic potential. The eigenstates of the field-free Hamiltonian were obtained in the form of Bloch states. The undisturbed crystal is assumed to be in thermal equilibrium, while initially the mid-IR field was described by a coherent state, and the HH modes are in their zero-photon states. The time evolution is governed by the von Neumann equation and solved using an appropriate Cash-Karp Runge-Kutta routine. Figure 1(a) shows a schematic of the interaction. Before the interaction, the laser field is in a coherent state [4,6]. In the high photon number limit, the photon-number probability distribution of this state (resulted by its projection to the photon number state) has a Gaussian form with its width reflecting the quantum noise of the light. A way to modify the quantum state of the light and its photon-number distribution is to use a process which depends nonlinearly on the instantaneous field amplitude [3,5,7,11,35–37]. In our case, the subcycle nonlinear process [Fig. 1(b)] which leads to HH generation changes the quantum state of the driving field and results in the generation of nonclassical light states having the photon-number distribution shown in Fig. 1(c). The properties of this quantum state are shown in phase space by the Wigner function $W(a)$, which, besides the squeezinglike effect, also depicts negative values

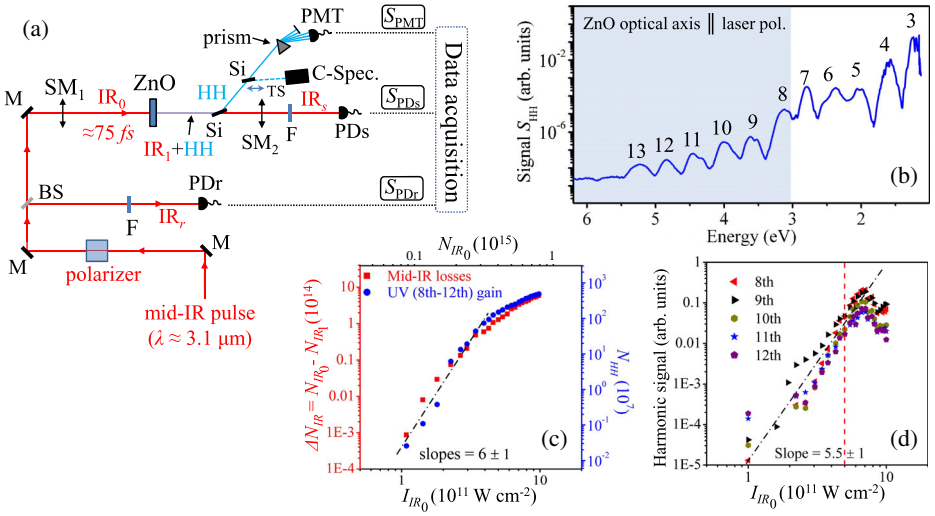

FIG. 2. (a) Experimental setup. M, mid-IR plane mirrors. Polarizer: A system of two polarizers used to control the laser pulse energy. BS, beam sampler used to reflect a small portion of the mid-IR beam towards the photodiode PD_r. SM_1, spherical focusing mirror of 50 cm focal length. IR_0, interacting mid-IR beam. IR_r, reference mid-IR beam. IR_1, mid-IR beam exiting the crystal. IR_s, mid-IR beam reaching the photodiode PD_s. SM_2, spherical focusing mirror used to collect the mid-IR beam on PD_s. HH, high-harmonic beam. Si, silicon plates used to reflect the harmonics towards the photomultiplier (PMT) and the conventional spectrometer (C-Spec). F, neutral density filters used for the attenuation of the mid-IR beam. (b) High-harmonic spectrum at the exit of the crystal recorded with C-Spec at $I_{IR_0} \approx 5 \times 10^{11}$ W cm^{-2} when the optical axis of the crystal is parallel to the laser polarization. (c) Dependence of the missing mid-IR photon number $\Delta N_{IR} = N_{IR_0} - N_{IR_1}$ (red points) and the generated UV photon number N_{HH} obtained by the PMT (blue points) at the exit of the crystal on I_{IR_0}. The upper x axis shows the photon number N_{IR_0} of the IR_0 beam. (d) Dependence of the harmonic signal on I_{IR_0} recorded by the conventional spectrometer. The black dashed lines show the linear fit on the raw data. The slopes depict the order of nonlinearity. The dashed red line shows the value of the I_{IR_0} used for the measurements of the mid-IR photon-number distribution.

[Fig. 1(d)]. The distribution in Fig. 1(c) consists of a series of peaks which correspond to the HH spectrum [Fig. 1(e)]. The peak structure appearing in the distribution ($P_n^{(abs)}$) of Fig. 1(c) is a quantum-optical effect which cannot be explained by semiclassical theories. It results from quantum interference of the mid-IR photons absorbed (with the periodicity of the laser field) towards UV emission and the projection of the final light state (generated with each shot) on photon-number states [35].

To measure the photon-number distribution, we have used the experimental setup shown in Fig. 2(a) (SM [30], Pts. 2 and 3). A laser system which delivers few-cycle mid-IR pulses at 100 kHz repetition rate was used [38]. A linearly polarized laser pulse (IR_0) of ≈3.1 μm carrier wavelength and ≈75 fs duration was focused into a 500-μm-thick ZnO crystal where harmonics were generated. For the measurement of the mid-IR photon statistics, we have used an IR_0 beam with photon number $N_{IR_0} \approx 4 \times 10^{14}$ photons per pulse and intensity on the crystal of $I_{IR_0} \approx 5 \times 10^{11}$ W cm^{-2}. The generated harmonic spectrum [Fig. 2(b)] was recorded by a conventional spectrometer, while the photomultiplier integrates the photon number of the harmonics generated mainly by interband transitions [20,21] (i.e., with photon energy >3.2 eV) without excluding the contribution of intraband dynamics in the generation of harmonics with photon energy <3.2 eV. The mid-IR beam exiting the crystal (IR_1), after being attenuated by a factor of $A \approx 3 \times 10^5$, was recorded by the photodiode PD_s. The signals of PD_r (S_{PDr}), PD_s (S_{PDs}), and photomultiplier (PMT) (S_{PMT}) were simultaneously recorded for each laser shot. S_{PDs} was used for recording the photon-number distribution of the mid-IR beam exiting the crystal, S_{PDr} for reducing the energy fluctuations of the laser, and S_{PMT} to correlate the harmonic signal with S_{PDs} and remove the unwanted background caused by processes irrelevant to the harmonic generation.

A key step towards the realization of the quantum-optical approach is the verification of the energy conservation and the nonlinearity of the interaction process. This was achieved by measuring the dependence of the missing mid-IR photon number $\Delta N_{IR} = N_{IR_0} - N_{IR_1}$ (where $N_{IR_1} = AN_{IR_s}^{(PD_s)}$ and $N_{IR_s}^{(PD_s)}$ is the mid-IR photon number exiting the crystal and reaching PD_s, respectively) and the generated UV photon number (N_{HH} measured by the PMT) at the exit of the crystal on I_{IR_0} [Fig. 2(c)]. It is evident that both ΔN_{IR} and N_{HH} have the same nonlinear dependence on I_{IR_0}. After an increase with slope of ≈6 ± 1, they saturate at $I_{IR_0}^{(sat)} \gtrsim 5 \times 10^{11}$ W cm^{-2}. This is in agreement with the dependence of the signal of the individual harmonics (measured by the conventional spectrometer) on I_{IR_0} in the nonperturbative regime [Fig. 2(d)]. The above clearly reflects the energy conservation and depicts that both ΔN_{IR}

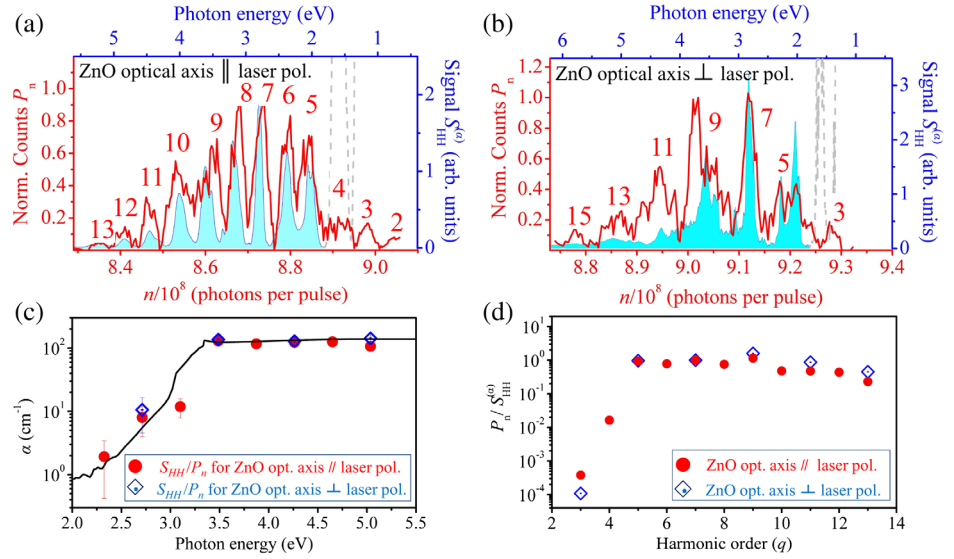

FIG. 3. (a),(b) Mid-IR harmonic spectra (red lines) and the conventional HH spectra (blue filled areas) recorded when the optical axis of the crystal was parallel and perpendicular to the laser polarization, respectively. The conventional HH spectra at the exit of the crystal obtained after taking into account the absorption coefficient of the crystal. (c) Measurement of the ZnO absorption coefficient. The black line shows the absorption coefficient of the ZnO crystal measured by conventional approaches. (d) Measurement of the contribution of the different harmonic generation mechanisms.

and N_{HH} originate from the same nonlinear interaction process.

To unravel the influence of the HH generation process on the state of the driving laser field, we have measured the photon-number distribution P_n of the mid-IR laser-field (named the "mid-IR harmonic spectrum") utilizing the detector PD_s and the "quantum spectrometer" approach [29]. The measured distribution [red line in Fig. 3(a)] is centered at $N_{\mathrm{IR}_s}^{(\mathrm{PD}_s)} \approx 8.70 \times 10^8$ photons per pulse and contains a series of confined peaks having a spacing of $\Delta N^{(q)}_{(\mathrm{IR}_{\mathrm{PD}_s})} = N^{(q-1)}_{(\mathrm{IR}_{\mathrm{PD}_s})} - N^{(q)}_{(\mathrm{IR}_{\mathrm{PD}_s})} \equiv \Delta N^{(q)}_{(\mathrm{IR})}/A \approx 6 \times 10^6$ photons per pulse. $N^{(q)}_{(\mathrm{IR}_{\mathrm{PD}_s})}$ is the corresponding to q photon-number reaching PD_s and $\Delta N^{(q)}_{(\mathrm{IR})}$ is the photon-number difference between consecutive q at the exit of the crystal. After finding the value of $N_{\mathrm{IR}_s}^{(\mathrm{PD}_s)}(q=0)$ (which reflects the remaining mid-IR photon number after the absorption due to processes other than harmonic emission, see Pt. 4 of SM [30]), the mid-IR photon number absorbed (i.e., missing photons) towards the harmonic emission is $N_{\mathrm{IR}_s}^{(\mathrm{PD}_s)}(q=0) - N^{(q)}_{(\mathrm{IR}_{\mathrm{PD}_s})}$. This number reflects the calculated $P_n^{(abs)}$ shown in Fig. 1(c). The distribution reveals the HH spectrum as (a) it exhibits a characteristic plateau and cutoff region, (b) the value of Δq measured by the mid-IR harmonic spectrum (SM [30], Pts. 4 and 5) is in agreement with the value expected from the process leading to the generation of the odd and even harmonics. i.e., $\Delta q \approx 1$, and (c) it is in agreement with the part of the HH spectrum (with $q > 4$) obtained by the conventional spectrometer [blue filled area in Fig. 3(a)] taking into account the absorption coefficient (α) of the ZnO crystal [39,40] [black solid line in Fig. 3(c)]. The above was confirmed by measurements performed when the ZnO crystal optical axis is perpendicular to the laser polarization [Fig. 3(b)]. In this case only the odd harmonics are emitted (SM [30], Pt. 6) [41] and the measured Δq is found to be ≈ 2. The latter constitutes the absolute validation check that the mid-IR harmonic spectrum reveals the HH spectrum.

The mid-IR harmonic spectra were used to measure the absorption coefficient of the crystal and determine the contribution of the different mechanisms participating in the HH generation process. Assuming that there are no data available about the absorption coefficient, its values can be obtained by dividing the harmonic signal of the conventional spectra [Fig. 2(b) and Fig. S5 of SM [30]] with the corresponding peak-normalized distribution of the mid-IR harmonic spectra, i.e., $\alpha = S_{\mathrm{HH}}/P_n$. The results [red points and blue rhombs in Fig. 3(c)] are found to be in fair agreement with the values obtained by conventional field-free approaches [black solid line in Fig. 3(c)]. The importance of this measurement relies on the capability of the approach to provide direct access to studies of optical properties of solids in the presence of strong fields [42].

To obtain the information about the mechanisms participating in the harmonic generation process, we compared the mid-IR harmonic spectrum with a conventional harmonic spectrum that has been corrected for the absorption $S^{(\alpha)}_{\mathrm{HH}}$. Figure 3(d) shows the ratio of the peaks of the mid-IR

harmonic spectra with the corresponding harmonic peaks of the conventional spectra ($P_n/S_{\mathrm{HH}}^{(\alpha)}$). While both are in agreement for harmonics with $q > 4$ ($P_n/S_{\mathrm{HH}}^{(\alpha)} \sim 1$), they depict a distinct difference for harmonics with $q < 5$ ($P_n/S_{\mathrm{HH}}^{(\alpha)} \sim 10^{-4}$). In this part of the spectrum, P_n drops by more than an order of magnitude compared to the plateau harmonics, while $S_{\mathrm{HH}}^{(\alpha)}$ in the conventional spectra increases by more than an order of magnitude. This is because the mid-IR harmonic spectrum results from the anticorrelation with the harmonics generated in the nonperturbative regime, a procedure (not achievable by conventional spectrometers) that eliminates the detection of harmonics generated by other processes like multiphoton absorption (SM [30], Pt. 3). The above is further supported by a recent theoretical model [21] where the harmonic spectra which have been calculated using interband transitions are in fair agreement with the mid-IR harmonic spectra shown in Figs. 3(a) and 3(b).

In conclusion, we demonstrate that strongly laser-driven semiconductors lead to the generation of nonclassical light states having subcycle electric field fluctuations that carry the information of the subcycle dynamics of the interaction. These states have been used to recover the high-harmonic spectrum, resolve the mechanisms participating in the high-harmonic emission, and measure the absorption coefficient of the crystal in the presence of strong laser fields. This work bridges the gap between quantum technology [2] and ultrafast optoelectronics and paves the way for the development of a new class of compact nonclassical light sources advancing studies ranging from quantum communication, information, and computation to high-precision interferometry applied to the detection of gravitational waves [2,11,43]. In addition, it opens up new ways for investigating strong-field interactions with other complex systems like molecules [44–47], nanostructures [48,49], and lower dimensional materials [50,51].

This work was supported by the LASERLAB-EUROPE (No. GA 654168), NFFA-Europe (No. 654360), "HELLAS-CH" (MIS 5002735) funded by the Operational Program (NSRF 2014-2020) and co-financed by Greece and the European Union, European Union's Horizon 2020 research and innovation program MEDEA (Marie Sklodowska-Curie Grant Agreement No. 641789), European Social Fund (EFOP-3.6.2-16-2017-00005). ELI-ALPS is supported by the European Union and co-financed by the European Regional Development Fund (GINOP-2.3.6-15-2015-00001). E. C. acknowledge support from the Institut Universitaire de France. We thank K. Osvay for his support during the experimental campaign at ELI-ALPS and D. Charalambidis for fruitful discussions. We also thank N. Papadakis for his technical support on the data analysis. N. T. was the main contributor in the experimental runs and data analysis; S. Kühn, M. D., S. Kahaly, and E. C. contributed to the experiment, data analysis, and manuscript preparation; P. F. and S. V. developed the theoretical model; B. K. was responsible for the operation of the mid-IR laser system; K. V. and I. A. G., contributed to the theoretical description of the HHG process; P. T. conceived and supervised the project, designed the experiment, and contributed to all aspects of the work.

*Corresponding author.
ptzallas@iesl.forth.gr

[1] M. Kira and S. W. Koch, *Semiconductor Quantum Optics* (Cambridge University Press, Cambridge, England, 2012).
[2] A. Acin, I. Bloch, H. Buhrman, T. Calarco, C. Eichler, J. Eisert, D. Esteve, N. Gisin, S. J. Glaser, F. Jelezko, S. Kuhr, M. Lewenstein, M. F. Riedel, P. O. Schmidt, R. Thew, A. Wallraff, I. Walmsley, and F. K. Wilhelm, New J. Phys. **20**, 080201 (2018).
[3] D. F. Walls, Nature (London) **306**, 141 (1983).
[4] R. Loudon, *The Quantum Theory of Light* (Oxford University Press Inc., New York, 2000).
[5] R. Loudon and P. L. Knight, J. Mod. Opt. **34**, 709 (1987).
[6] M. O. Scully and M. S. Zubairy, *Quantum Optics* (Cambridge University Press, Cambridge, England, 1997).
[7] G. Breitennbach, S. Schiller, and J. Mlynek, Nature (London) **387**, 471 (1997).
[8] U. L. Andersen, T. Gehring, C. Marquardt, and G. Leuchs, Phys. Scr. **91**, 053001 (2016).
[9] A. I. Lvovsky, in *Fundamentals of Photonics and Physics*, edited by D. L. Andrews (John Wiley & Sons Inc., New Jersey, 2015), Vol. I, p. 121.
[10] C. Riek, P. Sulzer, M. Seeger, A. S. Moskalenko, G. Burkard, D. V. Seletskiy, and A. Leitenstorfer, Nature (London) **541**, 376 (2017).
[11] R. Schnabel, Phys. Rep. **684**, 1 (2017).
[12] S. Y. Kruchinin, F. Krausz, and V. S. Yakovlev, Rev. Mod. Phys. **90**, 021002 (2018).
[13] T. T. Luu, M. Garg, S. Yu. Kruchinin, A. Moulet, M. Th. Hassan, and E. Goulielmakis, Nature (London) **521**, 498 (2015).
[14] M. Schultze, E. M. Bothschafter, A. Sommer, S. Holzner, W. Schweinberger, M. Fiess, M. Hofstetter, R. Kienberger, V. Apalkov, V. S. Yakovlev, M. I. Stockman, and F. Krausz, Nature (London) **493**, 75 (2012).
[15] M. Hohenleutner, F. Langer, O. Schubert, M. Knorr, U. Huttner, S. W. Koch, M. Kira, and R. Huber, Nature (London) **523**, 572 (2015).
[16] G. Vampa, T. J. Hammond, M. Taucer, X. Ding, X. Ropagnol, T. Ozaki, S. Delprat, M. Chaker, N. Thiré, B. E. Schmidt, F. Légaré, D. D. Klug, A. Yu. Naumov, D. M. Villeneuve, A. Staudte, and P. B. Corkum, Nat. Photonics **12**, 465 (2018).
[17] I. Floss, C. Lemell, G. Wachter, V. Smejkal, S. A. Sato, X.-M. Tong, K. Yabana, and J. Burgdörfer, Phys. Rev. A **97**, 011401(R) (2018).
[18] S. Ghimire, A. D. DiChiara, E. Sistrunk, P. Agostini, L. F. DiMauro, and D. A. Reis, Nat. Phys. **7**, 138 (2011).
[19] G. Vampa, C. R. McDonald, G. Orlando, D. D. Klug, P. B. Corkum, and T. Brabec, Phys. Rev. Lett. **113**, 073901 (2014).

[20] G. Vampa, T. J. Hammond, N. Thiré, B. E. Schmidt, F. Légaré, C. R. McDonald, T. Brabec, and P. B. Corkum, Nature (London) **522**, 462 (2015).
[21] E. N. Osika, A. Chacón, L. Ortmann, N. Suárez, J. A. Pérez-Hernández, B. Szafran, M. F. Ciappina, F. Sols, A. S. Landsman, and M. Lewenstein, Phys. Rev. X **7**, 021017 (2017).
[22] Z. Wang, H. Park, Y. H. Lai, J. Xu, C. I. Blaga, F. Yang, P. Agostini, and L. F. DiMauro, Nat. Commun. **8**, 1686 (2017).
[23] N. Tancogne-Dejean, O. D. Mücke, F. X. Kärtner, and A. Rubio, Phys. Rev. Lett. **118**, 087403 (2017).
[24] D. Golde, T. Meier, and S. W. Koch, Phys. Rev. B **77**, 075330 (2008).
[25] P. G. Hawkins, M. Yu. Ivanov, and V. S. Yakovlev, Phys. Rev. A **91**, 013405 (2015).
[26] G. Vampa, C. R. McDonald, G. Orlando, P. B. Corkum, and T. Brabec, Phys. Rev. B **91**, 064302 (2015).
[27] P. G. Hawkins and M. Yu. Ivanov, Phys. Rev. A **87**, 063842 (2013).
[28] T. Ikemachi, Y. Shinohara, T. Sato, J. Yumoto, M. Kuwata-Gonokami, and K. L. Ishikawa, Phys. Rev. A **95**, 043416 (2017).
[29] N. Tsatrafyllis, I. K. Kominis, I. A. Gonoskov, and P. Tzallas, Nat. Commun. **8**, 15170 (2017).
[30] See Supplemental Material at http://link.aps.org/supplemental/10.1103/PhysRevLett.122.193602 for details of the theoretical model, the quantum-optical nature of the "mid-IR harmonic spectrum," experimental approach, calibration of the "mid-IR harmonic spectra," mid-IR photon number estimation, and conventional high-harmonic spectrum at the exit of the spectrometer, which includes Refs. [31–34].
[31] J. von Neumann, *Mathematical Foundations of Quantum Mechanics* (Princeton University Press, Princeton, NJ, 1955).
[32] S. Jiang, J. Chen, H. Wei, C. Yu, R. Lu, and C. D. Lin, Phys. Rev. Lett. **120**, 253201 (2018).
[33] P. Földi, Phys. Rev. B **96**, 035112 (2017).
[34] P. Meystre and M. Sargent, *Elements of Quantum Optics*, 4th ed. (Springer, Berlin, 2007).
[35] I. A. Gonoskov, N. Tsatrafyllis, I. K. Kominis, and P. Tzallas, Sci. Rep. **6**, 32821 (2016).
[36] W. Schleich and J. A. Wheeler, Nature (London) **326**, 574 (1987).
[37] G. A. Garrett, A. G. Rojo, A. K. Sood, J. F. Whitaker, and R. Merlin, Science **275**, 1638 (1997).
[38] S. Kühn *et al.*, J. Phys. B **50**, 132002 (2017).
[39] J. F. Muth, R. M. Kolbas, A. K. Sharma, S. Oktyabrsky, and J. Narayan, J. Appl. Phys. **85**, 7884 (1999).
[40] V. Srikant and D. R. Clarke, J. Appl. Phys. **83**, 5447 (1998).
[41] S. Gholam-Mirzaei, J. Beetar, and M. Chini, Appl. Phys. Lett. **110**, 061101 (2017).
[42] S. Ghimire, A. D. DiChiara, E. Sistrunk, U. B. Szafruga, P. Agostini, L. F. DiMauro, and D. A. Reis, Phys. Rev. Lett. **107**, 167407 (2011).
[43] I. A. Walmsley, Science **348**, 525 (2015).
[44] T. Kanai, S. Minemoto, and H. Sakai, Nature (London) **435**, 470 (2005).
[45] S. Baker, J. S. Robinson, C. A. Haworth, H. Teng, R. A. Smith, C. C. Chirila, M. Lein, J. W. G. Tisch, and J. P. Marangos, Science **312**, 424 (2006).
[46] J. Itatani, J. Levesque, D. Zeidler, H. Niikura, H. Pepin, J. C. Kieffer, P. B. Corkum, and D. M. Villeneuve, Nature (London) **432**, 867 (2004).
[47] B. Wolter, M. G. Pullen, A.-T. Le, M. Baudisch, K. Doblhoff-Dier, A. Senftleben, M. Hemmer, C. D. Schröter, J. Ullrich, T. Pfeifer, R. Moshammer, S. Gräfe, O. Vendrell, C. D. Lin, and J. Biegert, Science **354**, 308 (2016).
[48] M. F. Ciappina *et al.*, Rep. Prog. Phys. **80**, 054401 (2017).
[49] S. Han, H. Kim, Y. W. Kim, Y.-J. Kim, S. Kim, I.-Y. Park, and S.-W. Kim, Nat. Commun. **7**, 13105 (2016).
[50] H. A. Hafez, S. Kovalev, J.-C. Deinert, Z. Mics, B. Green, N. Awari, M. Chen, S. Germanskiy, U. Lehnert, J. Teichert, Z. Wang, K.-J. Tielrooij, Z. Liu, Z. Chen, A. Narita, K. Müllen, M. Bonn, M. Gensch, and D. Turchinovich, Nature (London) **561**, 507 (2018).
[51] T. Higuchi, C. Heide, K. Ullmann, H. B. Weber, and P. Hommelhoff, Nature (London) **550**, 224 (2017).